Faraday Discussions

Cite this: DOI: 10.1039/d5fd00173k

PAPER

Competing reaction pathways in the decomposition of 2-propanol over V-doped Co_3O_4(111) model catalysts: a mechanistic study

Patrick Hubert, †[a] Jan Smyczek, †[a] Carsten Schröder, [a] Maximilian Galinski,[a] Lina M. Marquardt,[a] Justin Girschik,[a] Bernd Hartke, [a] Guntram Rauhut [b] and Swetlana Schauermann *[a]

Received 17th December 2025, Accepted 16th January 2026
DOI: 10.1039/d5fd00173k

We present a mechanistic study on selective alcohol decomposition over model cobalt oxide-based catalysts: pristine Co_3O_4(111)/Au(111) and Co_3O_4(111) containing different amounts and forms of vanadium oxide. These two types of model catalysts were prepared and investigated with respect to their structural and catalytic properties following a rigorous surface science approach under well-defined ultra-high vacuum (UHV) conditions employing a combination of scanning-tunnelling microscopy (STM), molecular-beam techniques, infrared reflection absorption spectroscopy (IRAS) and temperature programmed desorption (TPD). Upon vanadium deposition, three types of V-containing structures were identified on Co_3O_4(111): V atoms embedded into the Co_3O_4 lattice, and triangular two-dimensional (2D) and three-dimensional (3D) truncated triangular VO_x islands, whose relative abundance strongly depends on the amount of deposited V. Employing CO as a sensitive probe for adsorption sites, V atoms in different oxidation states were identified, including V^{3+}, V^{4+} and V^{5+} involved in vanadyl (V^{5+}=O) groups. The latter species were shown to participate in dissociation of 2-propanol to the propoxy reaction intermediate, likely serving as a H acceptor. The propoxy intermediate was found to dissociate to acetone on pristine Co_3O_4(111) and Co_3O_4(111) containing low V coverages, while increasing V loading leads to an alternative reaction pathway towards propene proceeding *via* C–O bond scission. Both the adsorbed reaction intermediate preceding propene formation and the gaseous product propene evolving above 430 K in TPD were detected for this reaction pathway. We discuss the possible reaction mechanisms of both competing reaction routes and connect them to the structure of different types of VO_x species.

[a]*Institute of Physical Chemistry, Christian-Albrechts-University Kiel, Max-Eyth-Str. 1, 24118 Kiel, Germany. E-mail: schauermann@pctc.uni-kiel.de*

[b]*Institute of Theoretical Chemistry, University of Stuttgart, Pfaffenwaldring 55, 70569 Stuttgart, Germany*

† Equal contribution.

Introduction

Heterogeneously catalysed selective dehydrogenation and dehydration of short-chain alcohols are important processes for technological applications aiming at feedstock chemicals.[1,2] Recently, oxide-based catalysts have been extensively investigated in this type of reactions and a special interest has arisen in transition metal oxides.[3–5] Promising catalysts, such as cobalt and vanadium oxides (VO_x) have been identified owing to their excellent performance, availability, stability and lower cost compared to noble metal catalysts.[2,6,7] Their catalytic properties can be tuned by modifying their composition, thereby enabling optimisation of the activity, stability and selectivity.[4,8]

Aiming at the atomistic-level understanding of the reaction mechanisms, several studies have been carried out on the spinel type cobalt oxide Co_3O_4 following a surface science approach under UHV conditions to investigate the decomposition of ethanol and 2-propanol to their corresponding aldehyde/ketone and water.[9,10] It was found that upon adsorption, ethoxy or propoxy species are formed as intermediates through deprotonation of the hydroxyl hydrogen ultimately resulting in aldehydes and ketones. Importantly, this reaction was shown to proceed *via* a Mars–van Krevelen mechanism consuming lattice oxygen atoms.[9,10]

Vanadium oxides are highly relevant for selective oxidation processes due to the multiple accessible oxidation states of vanadium (V^{3+}, V^{4+}, V^{5+}).[11–13] A combination of VO_x with other metal oxides, which has been recently explored in studies on powdered materials under technically relevant conditions,[14,15] potentially offers a promising way to improve the performance of such combined catalysts. Thus, supported VO_x catalysts exhibit high activity in the oxidative dehydrogenation of alkanes[15] or the oxidation of simple alcohols.[12,16–18] On reducible supports such as CeO_2 [13,15,16,18] or TiO_2,[19] VO_x catalysts exhibit higher conversion rates for oxidative dehydrogenation reactions, *e.g.* propane to propene or ethanol to acetaldehyde.[14,20,21] While the complex composition and structure of these combined oxide catalysts are advantageous for optimising their catalytic performance, this structural complexity hinders the understanding of structure–reactivity relationships and the rational design of new catalytic materials.

In our recent studies, a Co_3O_4(111)/Au(111) model catalyst and its powder counterpart were investigated in the decomposition of 2-propanol to acetone. The specific emphasis was on the effect of high temperature (573 K) pre-treatment with water, which was found to result in substantially higher catalytic activity as compared to pristine catalysts.[22] We attribute this improved catalytic behaviour to the formation of isolated surface hydroxyls involving lattice oxygen, which can effectively act as a hydrogen acceptor in 2-propanol deprotonation.[22]

To enhance the chemical complexity of this type of catalysts, we recently developed new model systems based on V incorporated into Co_3O_4(111) catalyst to model their powdered VO_x/Co_3O_4 counterparts, which were shown to lead to a different product distribution, including not only acetone but also propene.[23] These V-containing catalysts were comprehensively characterised by STM and IRAS employing CO as a probe molecule for different adsorption sites.[23] Specifically, three different VO_x-related structural motifs were identified and controllably prepared: (1) V atoms embedded into Co_3O_4(111) at the position of the regular

tetrahedral Co^{2+} sites, (2) 2D triangular VO_x islands containing one O–V layer and terminated by V^{3+} ions; and (3) extended 3D truncated triangular VO_x particles containing three V layers and terminated by V^{4+} atoms. Additionally, vanadyl (V^{5+}=O) groups were identified on these structures. Formation of these structures was found to depend on the V loading: while at low V coverages mostly embedded V atoms and 2D VO_x islands were observed, a higher amount of deposited V results in the formation of 3D VO_x islands.

In this study, we investigated the catalytic behaviour of these different types of $VO_x/Co_3O_4(111)$ catalysts in the decomposition of 2-propanol along competing pathways resulting in acetone and propene formation. Following a rigorous surface-science approach, we employed a combination of multimolecular beam techniques, IRAS, STM, TPD and theoretical computations, to address the elementary reaction steps and connect them with the structural properties of different VO_x species. Specifically, the vanadyl species were found to participate in 2-propanol dissociation to a propoxy intermediate, likely acting as hydrogen acceptors. This propoxy species decomposes to acetone on pristine $Co_3O_4(111)$ and at low V loadings, while higher V coverages enable an alternative pathway to propene *via* C–O bond cleavage.

Results and discussion

V-containing Co_3O_4 model catalysts were prepared based on well-defined $Co_3O_4(111)$ thin films epitaxially grown on Au(111) support, with V being deposited by physical vapor deposition on top of $Co_3O_4(111)$ films following by an oxidation step at elevated temperatures. The exact preparation procedure and experimental details are given in Chapter 1 of the SI. Their detailed structural characterization by STM and IRAS employing CO as a probe molecule is described elsewhere in more detail.[23] Here, we will only briefly summarize the major structural features, which are relevant for the further discussion. Fig. 1 displays the STM images and IRAS data obtained on these model surfaces for varying V loadings: pristine $Co_3O_4(111)$, and V-containing $Co_3O_4(111)$ with the V loadings 0.3, 0.6 and 0.9 monolayers (ML), with the monolayer being defined as the amount of V-atoms needed to form a layer of metallic V (2.3 Å), as measured using a quartz crystal microbalance (QCM).[24]

The series of IR spectra obtained for growing CO coverage on the reference surface – pristine $Co_3O_4(111)$/Au(111) – is shown in Fig. 1a, spectra series (4). These spectra exhibit a major vibrational mode observed at 2170 cm^{-1} for the lowest CO exposures, which red-shifts to 2158 cm^{-1} in saturation. An additional band is observed at 1748 cm^{-1} at higher CO coverages, which has been previously attributed to CO adsorbed at defect sites.[22,25,26] In Fig. 1e, a large scale STM image of the pristine $Co_3O_4(111)$/Au(111) is displayed revealing a well-defined surface morphology with large truncated bipyramidal islands averaging to 600–900 nm^2. In a close up STM image, a hexagonal unit cell with an interatomic distance of 5.7 $\pm$ 0.2 Å at an angle of 60 $\pm$ 1° can be identified. The corresponding LEED pattern also confirms a hexagonal symmetry pattern (see SI, Chapter 2).

The structure and morphology of epitaxially grown $Co_3O_4(111)$ ultrathin films have previously been reported on various substrates such as Ir(100),[27–29] Pd(100)[30] and Au(111),[22,31] which are terminated with tetrahedrally coordinated Co^{2+} ions exhibiting a closest Co–Co distance of 5.7 Å.[28,29] The IR studies of CO adsorbed as

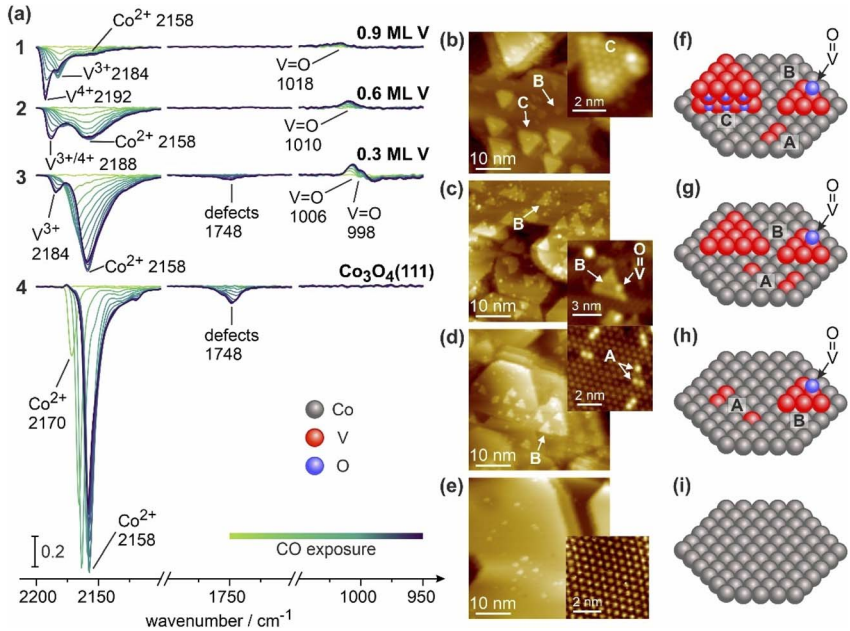

Fig. 1 (a) IRAS spectra of CO adsorption obtained on four types of surfaces: (spectra series 4) pristine Co_3O_4(111)/Au(111) and Co_3O_4(111) containing (3) 0.3 ML V, (2) 0.6 ML V and (1) 0.9 ML V at 100 K. STM images recorded on (e) pristine Co_3O_4(111)/Au(111) and Co_3O_4(111) containing (d) 0.3 ML V, (c) 0.6 ML V and (b) 0.9 ML V. See Chapter 10 in the SI for full experimental details. (f)–(i) Ball models of the identified structures.

a probe molecule for different sites showed the major band in the range of 2174–2158 cm^{-1} and a minor band evolving at high CO coverages at 1751–1743 cm^{-1},[25,26] which were assigned to CO adsorbed on the regular tetragonally coordinated Co^{2+} atoms and the defect sites, correspondingly.[25,26] The STM, IRAS and LEED measurements employed in our study are in excellent agreement with the reported literature data. Therefore, we conclude that the prepared oxide film is Co_3O_4(111) terminated with Co^{2+} ions.

Upon deposition of V onto the surface followed by oxidation at 650 K, pronounced changes in CO adsorption behaviour were observed. The IR spectra (3) (Fig. 1a) and the corresponding STM image (Fig. 1d) are related to the V coverage of 0.3 ML. The spectra exhibit a spectroscopic signature similar to the pristine surface with the main vibrational modes related to CO adsorbed on Co^{2+} (2170–2158 cm^{-1}) and at defect sites (1748 cm^{-1}). Their intensity, however, significantly decreases as compared to the pristine surface. In addition, a new band evolves at 2184 cm^{-1} and a negative band appears at 1006 cm^{-1} with a shoulder at 998 cm^{-1}. Upon increasing V coverage to 0.6 ML (Fig. 1a, spectra 2), the total IR intensity of CO adsorbed as Co^{2+} (band at 2158 cm^{-1}) further decreases with respect to pristine Co_3O_4(111), while the new CO vibrational band – now shifted to 2188 cm^{-1} – increases in intensity; the band at 1748 cm^{-1} disappears at this V coverage and the negative band shifts to 1010 cm^{-1}. At the highest V coverage, 0.9 ML (Fig. 1a, spectra 1), additional changes occur: a new distinct band evolves at 2192 cm^{-1} and becomes the most intense vibrational

mode, while the previously observed band at 2184 cm^{-1} persists as a pronounced shoulder. Notably, the vibration at 2158 cm^{-1}, formerly dominant, further decreases in intensity and the negative band further shifts to 1018 cm^{-1} and somewhat diminishes in intensity.

Fig. 1b–e show STM images corresponding to the discussed V coverages. It should be noted that the sample preparation for the STM and IRAS measurements has been performed in different chambers, so that the actual V coverages in STM can deviate from those reported for IRAS studies. In Fig. 1d, the STM image obtained at 0.3 ML V is shown, which exhibits two new structural features that were not visible on pristine $Co_3O_4(111)$, denoted as A and B. Species A appear as bright protrusions constituting of one, two or three atoms, exhibiting a height of 0.4 ± 0.2 Å. Species B form triangular shaped islands located both in the centre and at the edges of $Co_3O_4(111)$ terraces. These exhibit a height of 0.9 ± 0.2 Å and, additionally, some brighter protrusions at the edge or the corner of an B island with the height of 1.5 ± 0.2 Å. Fig. 1c shows the surface with a V coverage of 0.6 ML, on which the same type of species A and B were detected, however, here the total area of the species B has significantly increased by about factor of 3 as compared to the coverage of 0.3 ML, while the total concentration of the species A remains similar. With a further increasing V coverage to 0.9 ML, a new species C appears (Fig. 1b), which forms truncated triangular islands with a considerably greater height of 4.2 ± 0.4 Å. For this species, atomic resolution can be achieved on the top terrace, revealing an interatomic distance of 5.7 ± 0.2 Å.

Previously, growth and structural properties of well-defined V-containing model surface have been intensively investigated in surface science studies both for ultra-thin films of epitaxially grown vanadium oxides[24,32–44] and vanadium oxide clusters supported on other oxide films.[16–19,45] A comprehensive overview of these results is provided in Chapter 3 of the SI. Briefly, epitaxial growth of VO_x on metal single crystals (Au(111),[32–34] W(110),[35–37] Pd(111),[24,38–43] Rh(111)[46] and Pt(111)[44]) results in the formation of $V_2O_3(0001)$, typically terminated by the vanadyl (V^{5+}=O) groups exhibiting vibrational frequency in the range 1030–1040 cm^{-1} (ref. 47) and the height of approximately 2 Å as deduced from STM[46] and predicted by DFT.[42] CO adsorption on reduced $V_2O_3(0001)$ surfaces terminated by V^{3+} atoms gives rise to a vibrational band at 2166–2038 cm^{-1},[47] while CO adsorbed on V^{4+} – as measured on VO_x/Al_2O_3 powder catalysts – tends to exhibit higher vibrational frequencies up to 2212 cm^{-1}.[48] Note, however, that the reported vibrational ranges for V^{3+} and V^{4+} partly overlap.[47,48]

A large number of studies carried out on VO_x clusters supported on different oxide supports report similar vibrational frequencies both for the vanadyl groups and for CO adsorbed at V^{3+} and V^{4+} ions.[16–19,45,48] Table S1 and the related discussion in the Chapter 3 in the SI summarises these reported values for the available literature data.

Based on the combination of our experimental STM and IRAS data and the previous literature reports, we can assign the three different types of V-containing species observed in this study to particular structures (see Fig. 1b–e). First, there is a general trend: at the lowest and intermediate V coverage, only species A and B are populated as observed by STM, while their appearance coincides with the evolution of the new peak in IRAS at 2184 cm^{-1}, previously assigned to V^{3+} ions.[47–50] Increasing V loading from 0.3 to 0.6 ML results in a higher abundance of the species B, whose overall area increases by about factor of 3, while the total

amount of V atoms involved in the species A remains nearly constant. Second, at the highest investigated coverages (0.9 ML), the new species C evolve in the STM, whose appearance is correlated with the evolution of a new distinct band at 2192 cm^{-1}, which becomes the most prominent vibration. Simultaneously, the species A and B remain present on the surface, though at lower amounts as compared to the intermediate V coverage (0.6 ML). The band at 2184 cm^{-1} related to V^{3+} ions appears merely as a shoulder at this high V coverage. Overall, we observe a clear qualitative correlation between the appearance of the species A and B with the evolution of the band at 2184 cm^{-1} on the one hand and the appearance of the species C and the band at 2192 cm^{-1} on the other hand. Following the previous reports on vanadium oxides, in which V^{3+} and V^{4+} were proposed to co-exist as probed by adsorption of CO, we tend to assign the band at 2192 cm^{-1} to CO adsorbed at V^{4+} ions and the mode at 2184 cm^{-1} to CO residing at V^{3+} species. It should be noted, however, that this assignment should be taken with caution as the corresponding frequencies are very close and the appearance of two separated peaks might result in principle not from different oxidation states, but from *e.g.* strongly different geometric or electronic environments. Keeping in mind these possible complications, we will denote the corresponding states as V^{3+} and V^{4+} for simplicity, while the exact chemical state if these species must be resolved in upcoming XPS studies.

The bands appearing in the range 998–1018 cm^{-1} are situated in the vibrational range characteristic for vanadyl groups.[15,16,48] It should be, however, kept in mind that in our experimental setup we observed these bands in differential spectra resulting from CO adsorption. Most likely, these negative bands arise from the interaction of CO either directly with the vanadyl groups or with closely neighbouring metal atoms. This interaction likely shifts the actual vibrational band of the vanadyl group and leads to the evolution of the negative peaks detected in our differential spectra.

Combining these spectroscopic data with the results of STM, we can further refine the structural models of the species A, B and C, which are schematically displayed in Fig. 1f–i. The species A (height 0.4 ± 0.2 Å) can be assigned very likely to V atoms, which have replaced the regular tetrahedrally coordinated Co^{+2} atoms and by this become embedded into the surface lattice of $Co_3O_4(111)$. The measured interatomic distances between individual V atoms in dimers and trimers remain identical to the interatomic separation between Co^{2+} atoms in pristine $Co_3O_4(111)$ (5.7 Å). Species B exhibit a typical height of 0.9 ± 0.2 Å in STM, which is expected to be measured in STM as the height between the nearest O and V layers taking into account the typical V–O bond length of approximately 2 Å in V_2O_3 (refs. 33 and 34) and its inclination angle of 30° with respect to the surface plane as discussed in more detail elsewhere.[23] Taking into account the correlation between the growing amount of the species B and the enlargement of the IR band at 2184 cm^{-1} (V^{3+}), we assign these species to a single layer of VO_x, in which V atoms reside on top of the oxygen sublayer of the $Co_3O_4(111)$ support and exhibit the oxidation state V^{3+}. The brighter protrusions typically observed at the edges or corners of the species B match the theoretically predicted (1.57–1.61 Å)[33,34,42] and experimentally measured heights by IV-LEED (1.46 Å)[34] and STM (1.7–2.0 Å)[46,51] of the vanadyl (V═O) bonds, so that we can attribute these species to the vanadyl groups, appearing in the IR spectra in the range 998–1018 cm^{-1}.

Finally, the species C, exhibiting a typical height of 4.2 ± 0.4 Å, can be assigned to the extended three-dimensional (3D) islands containing three V layers (V–O–V–O–V) and terminated most likely by V^{4+} atoms, giving rise for adsorbed CO to a vibrational band at 2192 cm^{-1}.

The disappearance of the CO band related to the defects (1748 cm^{-1}) upon deposition of VO_x can be likely explained by the preferential nucleation of VO_x species at these sites.

Next, the catalytic activity in 2-propanol decomposition on well-defined $Co_3O_4(111)$/Au(111) and $VO_x/Co_3O_4(111)$/Au(111) model catalysts was investigated by a combination of TPD and IRAS. In order to discriminate between the fragmentation patterns of the reactant 2-propanol and the possible products acetone and propene, full range mass spectra were acquired for each molecule separately, which are shown in Fig. S2, Chapter 4 in the SI. Fig. 2 shows a series of TPD measurements performed following the exposure of 2-propanol at 100 K on pristine $Co_3O_4(111)$/Au(111) (Fig. 2a), and V-containing $Co_3O_4(111)$ model catalysts described above (Fig. 2b–d). Here, the masses of 2-propanol (45 amu) and the possible products water (18 amu), propene (41 amu) and acetone (43 amu) are shown in the temperature range of 150–650 K. It should be noted that the masses used to detect acetone (43 amu) and propene (41 amu) are present in the mass spectrum of 2-propanol as cracking fragments with relative intensities of 23% and 10%, respectively.

On pristine $Co_3O_4(111)$ (Fig. 2a) three principal 2-propanol desorption peaks are observed at around 200 K, 320 K and 400 K. Two main reaction products desorbing from this surface are acetone and water, while no formation of propene was recorded. The TPD trace of acetone shows a complex structure with multiple desorption peaks situated between 280 K and 450 K. Note that due to the presence

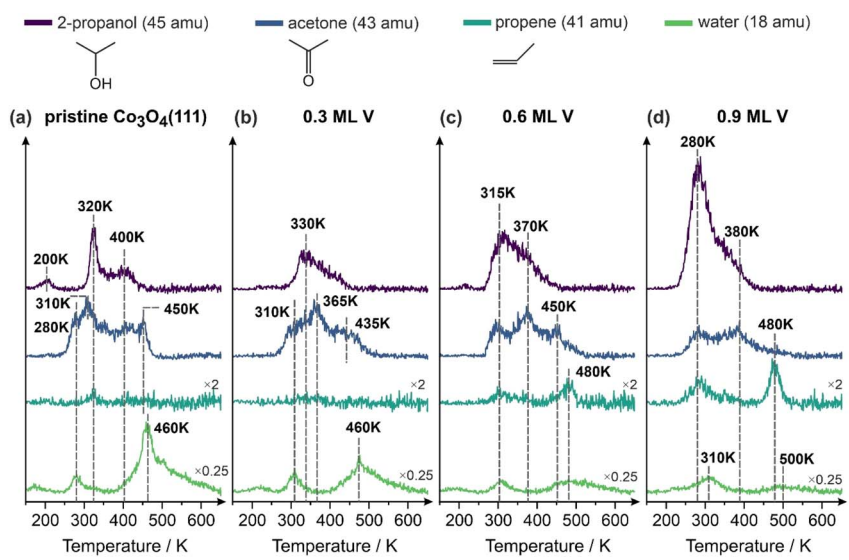

Fig. 2 TPD spectra obtained on (a) pristine $Co_3O_4(111)$ and $Co_3O_4(111)$ containing (b) 0.3 ML V, (c) 0.6 ML V and (d) 0.9 ML V following 2-propanol exposure (2.6×10^{14} molecules per cm^2) at 100 K.

of the cracking fraction of propanol in the mass 43 amu used to detect acetone, the overall intensity of the acetone signal appears higher in the range between 320 and 400 K. However, two acetone peaks at 280–310 K and 450 K do not overlap with desorbing 2-propanol and can be definitely ascribed exclusively to acetone formed in the reaction. The major water desorption peak at 460 K nearly coincides with the acetone peak at 450 K.

The adsorption and decomposition of 2-propanol over $Co_3O_4(111)$ model catalysts has already been studied comprehensively by using a combination of photoelectron spectroscopy (PES), STM and TPD by Libuda and co-workers.[10] After adsorption of 2-propanol at 150 K, PES experiments revealed that 2-propanol adsorbs both molecularly and dissociatively on $Co_3O_4(111)$ with the latter pathway resulting in the formation of propoxy species. The authors have concluded that molecular 2-propanol desorbs at 250 K, while the 2-propoxy species remain present up to 400 K and further decompose to acetone, desorbing from the surface above 420 K.[10] Based on the results of several consecutive TPD cycles, the authors proposed that this process is accompanied by formation of hydroxyl groups, which further transform to molecular water along a Mars-van Krevelen mechanism involving lattice oxygen.[10] More recently, we reported in a mechanistic study on the selective dehydrogenation of 2-propanol to acetone over $Co_3O_4(111)$, in which the promoting role of isolated surface hydroxyls for acetone formation was demonstrated.[22] Particularly, *operando* IRAS measurements revealed that 2-propoxy species and acetone readily form in the low-temperature pathway (180 K) after adsorption of 2-propanol at the surface containing isolated OH groups.[22]

Based on the assignment of Libuda *et al.*[10] and our own previous data,[22] we attribute the propanol TPD peak at 200 K observed in our study (Fig. 2a) to desorption of molecular 2-propanol and the peak at 400 K to recombinative propanol desorption. The low temperature pathway of acetone formation (280–310 K) can be likely explained by the above discussed low-temperature mechanism of 2-propanol dissociation involving isolated OH groups,[22] while the high temperature acetone formation route (450 K) can be assigned to deprotonation involving lattice oxygen and accompanied by water formation proposed by Libuda *et al.*[10] Note that since the concentration of isolated OH groups may substantially vary depending on the preparation conditions and water treatment,[22] the low-temperature acetone formation route (280–310 K) might be more pronounced on the $Co_3O_4(111)$ prepared in our study.

On $Co_3O_4(111)$ containing 0.3 ML of V (Fig. 2b), which exhibits the V-related species A and B, the reactivity behaviour of 2-propanol is quite similar – the propanol desorbs in the temperature range 290–450 K, while acetone and water appear as the major reaction products with the most dominant desorption peak at 365 K for acetone and at 460 K for water. Interestingly, the total amount of water desorbing in the high temperature range (460 K) decreases by about a factor of two as compared to pristine $Co_3O_4(111)$. No significant formation of propene was observed at this V coverage.

Also the surface covered with 0.6 ML of V (Fig. 2c) shows a similar trend with respect to acetone and water formation – both acetone and water are formed and desorb at similar temperatures or in a similar temperature range as on the pristine and V-containing (0.3 ML) $Co_3O_4(111)$. The trend of a decreasing amount of water desorbing above 460 K continues on this surface. There is, however,

a striking difference in the reactivity as compared to both previous catalysts – an onset of propene formation can be observed on this surface, with propene desorbing at 480 K (note that the small peak of 41 amu appears also at 315 K as a cracking fraction of 2-propanol). The same reactivity behaviour was also observed at $Co_3O_4(111)$ containing 0.9 ML of vanadium (Fig. 2d). Here, even smaller amounts of acetone are formed as compared to all previously discussed surfaces, but the propene signal (480 K) considerably increases in intensity. Only a negligible amount of water desorbs at 480–500 K – the pathway associated with water release involving lattice oxygen.

Overall, it can be concluded that the pristine $Co_3O_4(111)$ and $Co_3O_4(111)$ containing 0.3 ML of V catalyse the formation of acetone and water as the two major reaction products, whereas increasing V content leads to the formation of propene and strong attenuation of the acetone evolution.

In the next step, the surface species and reaction intermediates were investigated employing IRAS (Fig. 3 and 4). The spectra 1 and 2 in Fig. 3a are shown as representative spectra that were recorded following 2-propanol adsorption on pristine $Co_3O_4(111)$ at 180 K for different 2-propanol exposures: spectrum 1 corresponds to the initial stages of the reaction, spectrum 2 to the more advanced state. The evolution of different vibrational modes followed as a function of 2-propanol exposure as well as their detailed assignment have been comprehensively discussed in our recent publication[22] (see also Chapter 5 in the SI). Here, we will only briefly summarize the major observations that will be relevant for the further discussion. At 180 K, three surface species could be identified: (1) the reactant 2-propanol exhibiting the major vibrational band $\nu(C–O)_{Pr}$ at 972 cm^{-1},

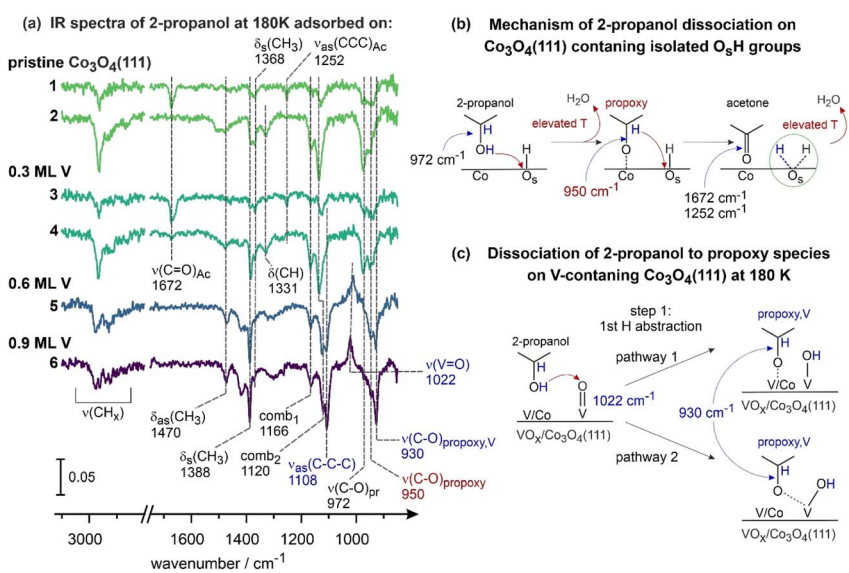

Fig. 3 (a) IR spectra of 2-propanol adsorbed at 180 K on (1 and 2) pristine $Co_3O_4(111)$ and $Co_3O_4(111)$ containing (3 and 4) 0.3 ML V, (5) 0.6 ML V and (6) 0.9 ML V (see Chapter 10 in the SI for full details). Proposed mechanisms of 2-propanol dissociation in the low-temperature regime at 180 K on (b) pristine $Co_3O_4(111)$ containing isolated O_sH and (c) on $Co_3O_4(111)$ containing vanadyl (V═O) groups.

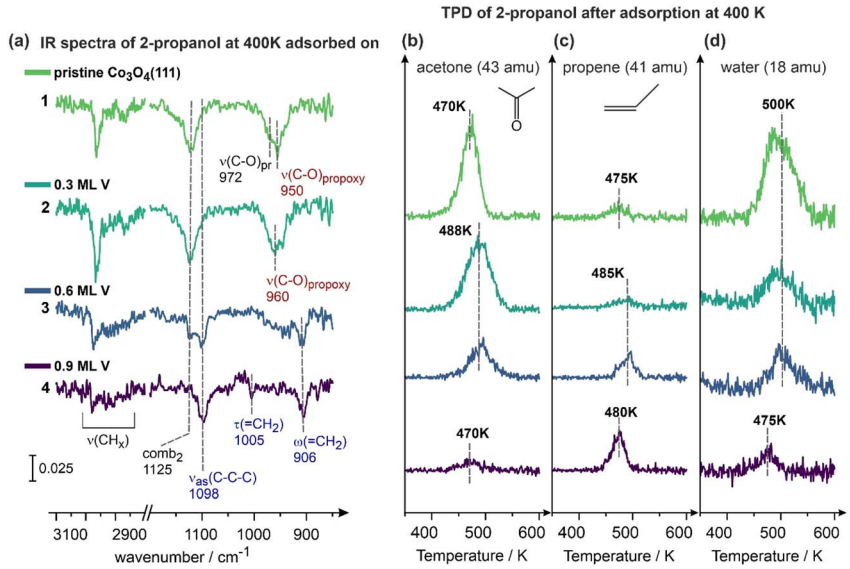

Fig. 4 (a) IR spectra obtained after deposition of 5.2×10^{14} molecules per cm^2 of 2-propanol at 400 K on (1) pristine $Co_3O_4(111)$ and $Co_3O_4(111)$ containing (2) 0.3 ML V, (3) 0.6 ML V and (4) 0.9 ML V. TPD spectra recorded after deposition of 2-porpanol at 400 K and cooling down to 100 K for (b) acetone, (c) propene and (d) water.

(2) the propoxy reaction intermediate showing the C–O stretching vibration $\nu(C–O)_{propoxy}$ at 950 cm^{-1} and (3) the target product acetone, which gives rise to the combination of the vibrational modes $\nu(C{=}O)_{Ac}$ at 1672 cm^{-1} and $\nu(CCC)_{Ac}$ at 1252 cm^{-1}. Importantly, the time evolution of these different species suggests that the propoxy reaction intermediate and the product acetone form readily already at 180 K (spectrum 1, Fig. 3a), when $Co_3O_4(111)$ contains isolated hydroxyl groups (O_sH, with O_s being a lattice oxygen atom of $Co_3O_4(111)$), which serve as an acceptor of H atoms abstracted from 2-propanol. In contrast, when all isolated O_sH groups are consumed in the course of the reaction, both half-dissociation steps stop, resulting in accumulation of the non-dissociated 2-propanol (972 cm^{-1}) and the propoxy species (950 cm^{-1}) as exemplarily shown in the spectrum 2 (Fig. 3a). Concomitantly, acetone formed at the earlier stages of the reaction desorbs resulting in vanishing of the associated vibrational bands at 1672 ($\nu(C{=}O)_{Ac}$) and 1252 cm^{-1} ($\nu(CCC)_{Ac}$). A comprehensive discussion on the proposed reaction mechanism occurring at the pristine $Co_3O_4(111)$ surface can be found elsewhere.[22] Fig. 3b shows the proposed reaction mechanism involving two half-dissociation steps on this surface and the isolated O_sH groups.

To assess the effects associated with the presence of various V-related structural features, adsorption and dissociation of 2-propanol was investigated *via* IRAS under identical conditions on all three types of surfaces described above (Fig. 3a, spectra 3–6). Here, we will discuss only the most relevant and abundant surface species and their changes as a function of V coverage. We refer the interested reader to Chapter 6 in the SI for the full set of spectra and their evolution recorded for systematically increasing 2-propanol exposures. On the surface containing 0.3 ML of V, the catalytic behaviour of 2-propanol closely

resembles the one observed on pristine $Co_3O_4(111)$: acetone (bands at 1672 and 1252 cm^{-1}) and the propoxy reaction intermediate (950 cm^{-1}) are readily formed at the initial stages of the reaction (spectrum 3). At higher 2-propanol exposures, both H abstraction steps become suppressed, resulting in the accumulation of non-dissociated 2-propanol (972 cm^{-1}) and the propoxy reaction intermediate (950 cm^{-1}), which was formed at the earlier states of the reaction but cannot dissociate further to acetone due to lack of O_sH groups. Molecular acetone, formed at the initial reaction stages, desorbs resulting in vanishing bands at 1672 and 1252 cm^{-1}. Other vibrational modes, such as the deformation and stretching vibrations of CH_x groups ($\delta_{as}(CH_3)$ at 1470 cm^{-1}, $\delta_s(CH_3)$ at 1368, 1388 cm^{-1}, $\nu(CH_3)$ in the range 2800–3000 cm^{-1}) and the combination modes at 1166 cm^{-1} and 1133 cm^{-1} ($comb_1$ ($\rho(CH_3 + \nu(C–C)$) and $comb_2$ ($\rho(CH_3 + \nu(C–O)$, respectively), remain largely unchanged as compared to the case of pristine $Co_3O_4(111)$. Based on these observations, it can be concluded that the chemistry of 2-propanol on this surface is dominated by $Co_3O_4(111)$ and the deposited V does not exhibit any noticeable effect at the product formation.

The spectra 5 and 6 in Fig. 3a are related to the higher formal V coverages of 0.6 and 0.9 ML, respectively. Note that for clarity reasons only the spectra related to high 2-propanol exposures are displayed here, which happen to be representative of the entire 2-propanol exposure range (see Chapter 6 in the SI for the full spectra series for systematically increasing 2-propanol exposures).

For the V coverage of 0.6 ML, substantial changes in the distribution of vibrational bands can be detected: a new band at 930 cm^{-1} evolves, which lies close to the band at 950 cm^{-1} related to the propoxy species ($\nu(C–O)_{propoxy}$) formed at $Co_3O_4(111)$ and in the typical range of C–O stretching vibrations.[5] Based on the similarity of the vibrational frequencies, we assign this band to the C–O stretching vibration of the propoxy species formed on the V-containing surface, $\nu(C–O)_{propoxy,V}$. In the following, we will denote this new propoxy group as propoxy, V species. Importantly, the band at 950 cm^{-1} related to the propoxy reaction intermediate formed on pristine $Co_3O_4(111)$ is still seen on this surface as a shoulder of the band at 930 cm^{-1}. Additionally, a new intense band evolves at 1108 cm^{-1}, lying in the typical range for skeletal C–C–C stretching vibrations of 2-propanol,[22,52] $\nu_{as}(C–C–C)$, which partly overlaps with the combination mode $comb_2$ ($\rho(CH_3 + \nu(C–O)$) of 2-propanol at 1133 cm^{-1}. Another striking observation is related to the evolution of the negative band at 1022 cm^{-1}, which is likely indicative of the depletion of the vanadyl (V=O) groups occurring in the course of the reaction. The intensity of the vibrational bands related to the CH_x deformation vibrations (($\delta_{as}(CH_3)$ at 1470 cm^{-1} and $\delta_s(CH_3)$ at 1388 cm^{-1}) somewhat increases as compared to the lower V coverage (0.3 ML), however, the intensity distribution between the symmetric (1388 cm^{-1}) and the asymmetric (1470 cm^{-1}) modes does not undergo notable changes. It should be emphasized that on this surface containing 0.6 ML of V, no acetone formation was detected at any applied 2-propanol exposure.

A very similar evolution of the surface species in the course of the reaction was also detected for $Co_3O_4(111)$ containing 0.9 ML of V (spectrum 6 in Fig. 3a). Here, the changes related to the presence of V species become even more pronounced: the new band at 930 cm^{-1} ($\nu(C–O)_{propoxy,V}$) further gains in intensity, the band associated with propoxy species formed on regular $Co_3O_4(111)$ surface, $\nu(C–O)_{propoxy}$ at 950 cm^{-1}, completely vanishes, the new band at 1108 cm^{-1} (ν_{as}(C–C–

C)) additionally gains in intensity as well as the negative band at 1022 cm^{-1} related to the vanadyl groups. Importantly, also at this V coverage, no acetone formation was observed in the entire applied range of 2-propanol coverages.

Overall, a very clear trend could be observed based on the population of surface species evolving at 180 K: while in pristine $Co_3O_4(111)$ and $Co_3O_4(111)$ containing 0.3 ML of V, acetone formation can be detected spectroscopically, the $Co_3O_4(111)$ catalysts containing 0.6 and 0.9 ML of V, show a clearly different reactivity: no acetone is formed and the reaction intermediate propoxy species exhibits a clearly different vibration frequency $\nu(C–O)_{propoxy,V}$, which is observed to be red shifted by 20 cm^{-1} as compared to pristine $Co_3O_4(111)$. This observation likely suggests that the propoxy, V species is formed either directly on V or in the immediate vicinity of a V atom. Additionally, the negative vibrational band associated with the vanadyl groups indicates that the latter species are involved in the decomposition of 2-propanol.

The combination of these observations can be interpreted as a new reaction pathway of 2-propanol decomposition opening up on the V-containing surfaces and involving the vanadyl groups. Indeed, this new reaction pathway can be also deduced from the reactivity data obtained by TPD (Fig. 2): while the pristine $Co_3O_4(111)$ and $Co_3O_4(111)$ containing 0.3 ML of V catalyze exclusively acetone formation, the same $Co_3O_4(111)$ surface containing 0.6 and 0.9 ML of V was shown to produce propene as a new reaction product. Additionally, some acetone was found to be formed as a second product, however, it's yield was found to decrease with increasing V content. Combining both observations, it can be concluded that the onset of propene formation as a gaseous product is correlated to the appearance of all new vibrational features observed on the surfaces containing 0.6 and 0.9 ML of V (see the vibrational modes marked with blue color in the Fig. 3a).

It is important to emphasize, however, that the mechanism of propene formation involving the reaction intermediate deduced from the IR spectra (propoxy species) must contain also further elementary reaction steps. Indeed, while 2-propanol decomposition to acetone on pristine $Co_3O_4(111)$ (see the scheme shown in Fig. 3b) involves only two H abstraction steps forming the propoxy species as the reaction intermediate (band at 950 cm^{-1}) and acetone as the product (bands at 1672 and 1252 cm^{-1}), which could be identified spectroscopically in our studies, decomposition of 2-propanol to propene must include also the scission of the C–O bond resulting in some new reaction intermediate, which was not detected so far at 180 K. Based on the correlation between the evolution of the new propoxy species associated with V (band at 930 cm^{-1}, $\nu(C–O)_{propoxy,V}$) and formation of propene in the gas phase (TPD, Fig. 2), we believe that the C–O bond scission occurs very likely in this new intermediate. Additionally, taking into account the fact that formation of the propoxy, V intermediate is accompanied by the consumption of the vanadyl species, it can be hypothesised that the V^{5+}=O groups act as a hydrogen acceptor during dissociation of 2-propanol to the propoxy, V intermediate. The scheme shown in Fig. 3c displays the possible scenarios how this process can occur in V-containing surfaces. Note that it takes into account two facts: (1) the newly formed propoxy, V species must be situated either directly on or in the close vicinity of a V atom, since it appears in IR red-shifted by 20 cm^{-1} as compared to the regular propoxy species formed on the Co^{2+} atoms of $Co_3O_4(111)$, and (2) the vanadyl

groups become consumed in this process, *e.g.* the abstracted H atom is transferred directly to the vanadyl group.

In order to further investigate the decomposition process of the new formed propoxy, V reaction intermediate to propene over V-containing $Co_3O_4(111)$, we performed IR measurements under temperature conditions that are closer to the temperature range in which propene desorbs from the surface as deduced from TPD (430–530 K, see Fig. 2). Fig. 4a displays the IR spectra obtained after exposure of model catalysts to 2.5 L of propanol at 400 K – the temperature is potentially high enough to induce the C–O bond scission, however, the resulting reaction intermediate is still expected to remain adsorbed on the surface and detected by IRAS. The spectra were recorded on pristine $Co_3O_4(111)$, spectrum 1, and V-containing $Co_3O_4(111)$ with the same V coverages as discussed above 0.3, 0.6 and 0.9 ML, spectra 2–4, correspondingly. Here, only the most relevant spectral regions are displayed, while the respective full spectra can be found in Chapter 7 in the SI. Fig. 4b displays the TPD signals obtained after the IR spectra were recorded at 400 K and the sample was cooled down to 100 K for TPD.

The spectra 1 and 2 (Fig. 4a), related to pristine $Co_3O_4(111)$ and $Co_3O_4(111)$ containing 0.3 ML V, exhibit very similar vibrational signatures: the intense broad band at 950–960 cm^{-1}, lying in the range of C–O stretching vibrations and related to the regular propoxy groups formed at the $Co_3O_4(111)$ surface. Note that on the pristine surface a shoulder at 972 cm^{-1} is also visible, which is related to non-dissociated 2-propanol that apparently remains present in small amounts also at 400 K, likely on some strongly bonding sites, *e.g.* surface defects. The second very prominent vibration on these two surfaces is the combination mode $comb_2$ ($\rho(CH_3) + \nu(C–O)$) evolving at 1125 cm^{-1}, which was also observed at 180 K at all investigated surfaces (Fig. 3a).

Interestingly, at higher V coverages – 0.6 and 0.9 ML – the bands related to the propoxy groups completely vanish (spectra 3 and 4, Fig. 4a) and a new band at 906 cm^{-1} appears, gaining in intensity with increasing V content. Additionally, a new band at 1098 cm^{-1} evolves at these two surfaces and also gains in intensity with growing V coverage. Additionally, both spectra recorded for higher V contents of 0.6 and 0.9 ML do not show the combination mode $comb_2$ ($\rho(CH_3) + \nu(C–O)$) that was visible at 1125 cm^{-1} on pristine Co_3O_4 and the surface with the lowest V coverage (0.3 ML). The absence of this latter band, containing a contribution from the ν(C–O) mode, as well as the absence of any type of propoxy groups indicate that a bond scission of the C–O bond occurs at this temperature.

The new band at 1098 cm^{-1} shows great similarity with the band at 1108 cm^{-1} evolving after 2-propanol adsorption at 180 K (see IR spectra 5 and 6 displayed in Fig. 3a): it is close in frequency, and appears only at both highest V coverages – 0.6 and 0.9 ML, *i.e.* it must be also related to the presence of large amount of V atoms. Based on these similarities, we assign this band to the same vibrational mode – asymmetric skeletal stretching ν_{as}(C–C–C) vibration. The other new vibration – the band at 906 cm^{-1} – was not observed at 180 K (Fig. 3a).

The TPD traces obtained directly after deposition of 2-propanol at 400 K (Fig. 4b–d) show a very clear trend: while on the pristine $Co_3O_4(111)$ and $Co_3O_4(111)$ containing 0.3 ML of V the major products are acetone and water, growing V content (0.6 and 0.9 ML of V) leads to the shift of the product distribution towards propene, while the amounts of formed acetone and water gradually decrease.

Overall, the evolution of two new vibrational bands at 906 cm^{-1} and 1098 cm^{-1} appearing and gaining in intensity with growing V coverage strongly correlate with the formation of propene as the gaseous reaction product as observed by TPD. For this reason, it can be hypothesized that these two bands are related to the surface reaction intermediate(s) leading to propene. In fact, vibrational bands in the range 908–924 cm^{-1}, which lies close to the experimentally observed value 906 cm^{-1}, were previously reported for propene adsorbed in various types of single crystals, such as Ag(111),[53] Cu(111)[54] and Au(111)[55] and in the gas phase[56,57] and assigned to the wagging vibration of the methylene group $\omega(=CH_2)$.

In order to verify this previous assignment, we performed a theoretical calculation of the propene IR spectrum in the gas phase and compared it to the experimentally measured spectrum of propene adsorbed in Au(111) at 100 K (Fig. 5). The latter metal was chosen as an inert reference, at which propene is not expected to undergo strong chemical transformations at 100 K and its experimental vibrational spectrum can be therefore compared to the computed one. For comparison, propene was also adsorbed at the Co_3O_4(111) surface containing 0.9 ML of V. Fig. 5 displays the theoretically computed (spectrum 1) and experimentally measured (spectrum 2 on Au(111) and spectrum 3 on 0.9 ML V/Co_3O_4(111)) vibrational spectra of propene. For the detailed discussion of the vibrational bands appearing in the relevant region close to 1000 cm^{-1} the interested reader is referred to the SI, Chapter 8, Fig. S12–15 and Table S3 in the SI summarizes all computed results as well as their assignments. The full assignments of all the experimentally measured modes of propene and the corresponding spectra can be found in Chapter 9 in the SI. Briefly, the experimental spectrum obtained for the nearly unperturbed propene adsorbed on Au(111) exhibits the following major vibrations: $\nu_{as}(CH_3)$ at 2925 cm^{-1}, the ν(C=C) at 1628 cm^{-1}, the $\delta_{as}(CH_3)$ at 1427 cm^{-1}, $\tau(=CH_2)$ at 981 cm^{-1} and the $\omega(=CH_2)$ vibration at 907 cm^{-1}. The experimentally observed vibrations are in excellent agreement with the results reported on Au(111) using HREELS.[55] Here, we will only focus on the fact, that the band experimentally observed at 906 cm^{-1} on 0.9 V/Co_3O_4(111) (spectrum 3, Fig. 5) largely coincides with the band at 907 cm^{-1} ($\omega(=CH_2)$) detected on Au(111) and can be indeed most likely assigned to the

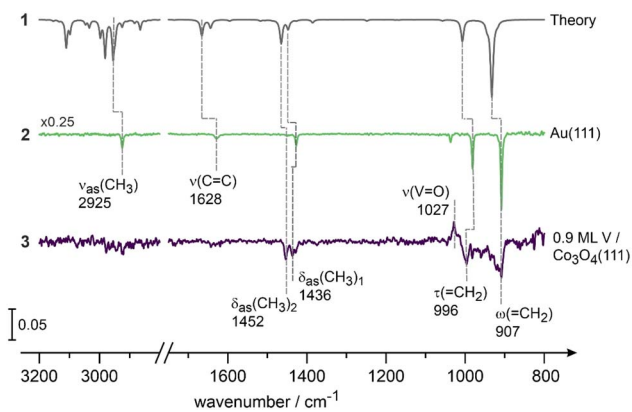

Fig. 5 (1) Calculated and experimental IR spectra of propene (5.2×10^{14} molecules per cm^2) adsorbed on (2) Au(111) and (3) Co_3O_4(111) containing 0.9 ML V measured at 100 K.

wagging vibration of the methylene group $\omega(=CH_2)$. Interestingly, no skeletal asymmetric stretching vibration (ν_{as}(C–C–C)) is detected in molecular propene itself.

Thus, the evolution of the band at 906 cm^{-1} observed on Co_3O_4(111) surfaces containing high concentrations of V (0.6 and 0.9 ML) is in principle consistent with formation of propene as a reaction product. However, the molecular form of propene is unlikely to reside on the surface at 400 K, as desorption temperatures of olefins are typically significantly lower and lie in the range 160–290 K as was reported on V_2O_3(0001), Ag(111) and Au(111);[12,53,55] for this reason, the band at 906 cm^{-1} is likely related to a reaction intermediate containing the terminal C=C double bond, which is, however, still covalently bonded to the underlying V atom. Our experimental spectroscopic data do not allow us to deduce a more precise structure of this intermediate. However, the most important structural features can be summarized as follows: (1) the reaction intermediate does not contain the C–O single bond as evidenced by the absence of the bands related to the C–O stretching vibration in the propoxy species (930 cm^{-1}) as well as the combination band comb$_2$ ($\rho(CH_3) + \nu$(C–O)) containing the contribution from the C–O bond; (2) it contains the terminal methylene group ($=CH_2$) as evidenced by the appearance of the band at 906 cm^{-1} related to the wagging $\omega(=CH_2)$ vibration; and (3) it is strongly bonded to the surface, *e.g. via* establishing a covalent bond between one of the C atoms to the underlying V atom, as in the opposite case the molecular form of propene is expected to desorb at lower temperatures than observed experimentally. Fig. 6 displays a possible structure (S_1) of this reaction intermediate, which is consistent with all experimental observations. Note that the band related to the $\tau(=CH_2)$ vibrational mode (996–1005 cm^{-1}, appearing at high V coverages in the spectrum 4, Fig. 4a and the spectrum 3, Fig. 5) is also consistent with the proposed reaction intermediate S_1 containing the terminal methylene ($=CH_2$) group. In this reaction mechanism, the propoxy, V group ($\nu(C–O)_{propoxy,V}$, 930 cm^{-1}) formed at the earlier stages of 2-propanol decomposition undergoes C–O bond scission resulting in the formation of the reaction intermediate S_1, containing a C=C double bond ($\omega(=CH_2)$, 906 cm^{-1} and $\tau(=CH_2)$, 996–1005 cm^{-1}). This reaction intermediate is covalently bound to the surface and – after H

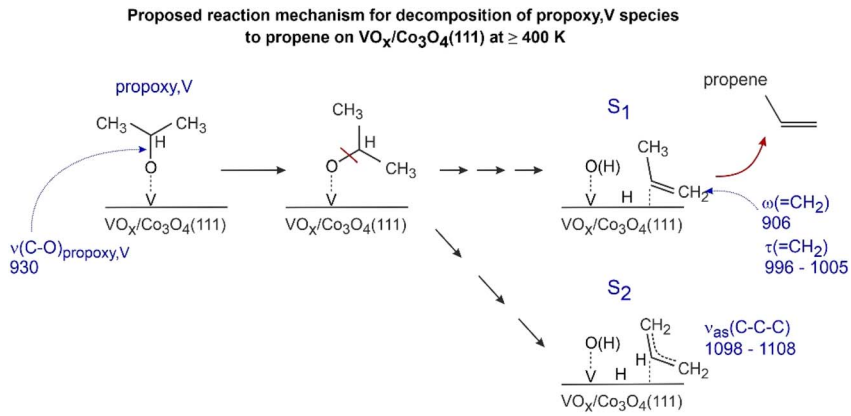

Fig. 6 Proposed reaction mechanism for decomposition of propoxy, V species to propene on VO_x/Co_3O_4(111)/Au(111) in the high temperature regime (≥400 K).

insertion into the surface-C bond – can desorb into the gas phase as propene. It should be also noted that a second prominent surface species characterized by the vibrational band at 1098–1108 cm^{-1}, ν_{as}(C–C–C), appears at 400 K after 2-propanol adsorption at surfaces containing high V coverages. Note that this band is not present in molecular propene and therefore is most likely related to a different surface species containing multiple C atoms but no C–O bond. One of the possible structures of this species is proposed in Fig. 6 as the species S_2. It should be considered, however, as a best guess and not as a spectroscopically well-confirmed species.

Finally, a clear correlation between the structure of the V-containing surfaces and their catalytic performance can be drawn: (1) the combination of the species A (embedded V atoms) and B (2D islands terminated by V^{3+}), appearing at low V coverage (0.3 ML), show a catalytic performance similar to that of Co_3O_4(111), *i.e.* the surface chemistry is most likely dominated by cobalt oxide; (2) at higher V coverages on the surfaces containing a large amounts of species C (3D islands exhibiting V^{4+} atoms) and vanadyl groups, propene formation is observed, which proceeds *via* the deprotonation of 2-propanol to propoxy, V species involving vanadyl groups and C–O bond scission resulting in the S_1 reaction intermediate. It should be also noted that while this work establishes a clear correlation between the presence of particular V-related structures and catalytic selectivity, it does not yet finally resolve all details of the atomic scale mechanism. A comprehensive theoretical study is required to compute the barrier heights and energy minima along the proposed reaction pathways for all relevant V-containing structures. These studies are now being performed and will be subject of upcoming publications.

Conclusions

Summarising, we report a mechanistic study on the structural properties and catalytic activity of VO_x incorporated into a well-defined Co_3O_4(111)/Au(111) model catalyst prepared and characterized following a rigorous surface science approach by a combination of STM, IRAS, TPD and molecular beam techniques. We identified three distinct types of VO_x species formed upon vanadium deposition followed by oxidation at elevated temperatures: isolated V atoms incorporated into the Co_3O_4(111) lattice, 2D triangular VO_x islands, and 3D VO_x aggregates. Their relative abundance is governed by V loading and determines the distribution of V oxidation states (V^{3+}, V^{4+}, and V^{5+} in vanadyl (V^{5+}=O) groups), as confirmed by CO adsorption experiments. The latter species were shown to participate in the dissociation of 2-propanol to the propoxy reaction intermediate on surfaces containing high V loadings, most likely serving as an efficient H acceptor. Spectroscopically, it was possible to differentiate between the propoxy intermediate formed at the regular Co^{2+} centres and the propoxy, V species, which are formed directly on or in close vicinity of V. The propoxy intermediate were found to dissociate to acetone on pristine Co_3O_4(111) and Co_3O_4(111) containing low V coverages, while increasing V loading leads to an alternative reaction pathway towards propene proceeding *via* C–O bond rupture. Both the adsorbed reaction intermediate preceding propene formation as well as the gaseous product propene evolving above 430 K in TPD were detected for this reaction pathway. We propose possible reaction mechanisms for both competing reaction

routes. Overall, the results establish a clear structure–reactivity relationship, demonstrating that specific VO_x motifs evolving at higher V loadings induce the C–O bond splitting in 2-propanol resulting in propene formation.

Conflicts of interest

There are no conflicts to declare.

Data availability

The data supporting the findings of this study are available within the article and its supplementary information (SI). Additional data are available from the corresponding author upon reasonable request. Supplementary information: experimental section; STM image and LEED pattern of $Co_3O_4(111)$/Au(111); extended summary of the literature data available for the model $Co_3O_4(111)$ and different types of vanadium oxide; fragmentation pattern of 2-propanol, acetone and propene; fragmentation pattern of 2-propanol, acetone and propene; full sets of IR spectra shown in Fig. 4 of the manuscript; calculation of IR spectra of propene; full IR spectra of propene adsorbed on $Co_3O_4(111)$ containing 0.9 ML V at 100 K and vibrational assignment of the IR spectra of propene on Au(111) and $Co_3O_4(111)$ containing 0.9 ML V. See DOI: https://doi.org/10.1039/d5fd00173k.

Acknowledgements

Financial support by the Deutsche Forschungsgemeinschaft (DFG, German Research Foundation; Project-ID 388390466 – TRR 247 ("Heterogeneous Oxidation Catalysis in the Liquid Phase")) is gratefully acknowledged. This research was supported in part through high-performance computing resources available at the Kiel University Computing Centre. We thank Philipp A. Fredersdorff and Paul Fröhlich for helpful discussions.

References

1 M. Cozzolino, R. Tesser, M. Diserio, P. Donofrio, *et al.*, *Catal. Today*, 2007, **128**, 191.
2 S. Najafishirtari, K. Friedel Ortega, M. Douthwaite, *et al.*, *Chem. – Eur. J.*, 2021, **27**, 16809.
3 H. Kuhlenbeck, S. Shaikhutdinov and H. J. Freund, *Chem. Rev.*, 2013, **113**, 3986.
4 S. Sahoo, K. Y. Wickramathilaka, E. Njeri, D. Silva, *et al.*, *Front. Chem.*, 2024, **12**, 1374878.
5 M. K. Weldon and C. M. Friend, *Chem. Rev.*, 1996, **96**, 1391.
6 S. Anke, G. Bendt, I. Sinev, H. Hajiyani, H. Antoni, *et al.*, *ACS Catal.*, 2019, **9**, 5974.
7 B. M. Weckhuysen and D. E. Keller, *Catal. Today*, 2003, **78**, 25.
8 T. P. Mabate, N. P. Maqunga, S. Ntshibongo, M. Maumela, *et al.*, *SN Appl. Sci.*, 2023, **5**, 196.
9 S. Reindl, J. Škvára, J. Hauner, A. Simanenko, *et al.*, *ChemCatChem*, 2024, **17**, e202401587.

10 C. Hohner, M. Ronovský, O. Brummel, T. Skála, *et al.*, *J. Catal.*, 2021, **398**, 171.
11 P. Hu, P. Hu, T. D. Vu, M. Li, *et al.*, *Chem. Rev.*, 2023, **123**, 4353.
12 A. Bandara, M. Abu-Haija, F. Höbel, H. Kuhlenbeck, *et al.*, *Top. Catal.*, 2007, **46**, 223.
13 J. M. Vohs, T. Feng and G. S. Wong, *Catal. Today*, 2003, **85**, 303.
14 B. Beck, M. Harth, N. G. Hamilton, C. Carrero, *et al.*, *J. Catal.*, 2012, **296**, 120.
15 L. Schumacher, J. Weyel and C. Hess, *J. Am. Chem. Soc.*, 2022, **144**, 14874.
16 H. L. Abbott, A. Uhl, M. Baron, Y. Lei, *et al.*, *J. Catal.*, 2010, **272**, 82.
17 L. Artiglia, S. Agnoli and G. Granozzi, *Coord. Chem. Rev.*, 2015, **301–302**, 106.
18 T. Feng and J. M. Vohs, *J. Catal.*, 2004, **221**, 619.
19 S. Agnoli, M. Sambi, G. Granozzi, C. Castellarin-Cudia, *et al.*, *Surf. Sci.*, 2004, **562**, 150.
20 A. Khodakov, B. Olthof, A. T. Bell and E. Iglesia, *J. Catal.*, 1999, **181**, 205.
21 A. Dinse, B. Frank, C. Hess, D. Habel, *et al.*, *J. Mol. Catal. A: Chem.*, 2008, **289**, 28.
22 J. Smyczek, P. Hubert, H. Scheele, C. Schröder, *et al.*, *ACS Catal.*, 2025, **15**, 19268.
23 J. Smyczek, P. Hubert, H. Scheele, C. Schröder *et al.*, Submitted.
24 S. Surnev, L. Vitali, M. G. Ramsey, F. P. Netzer, *et al.*, *Phys.Rev.B:Condens. Matter Mater. Phys.*, 2000, **61**, 13945.
25 P. Ferstl, S. Mehl, M. A. Arman, M. Schuler, *et al.*, *J. Phys. Chem. C*, 2015, **119**, 16688.
26 G. Fickenscher, C. Hohner, T. Xu and J. Libuda, *J. Phys. Chem. C*, 2021, **125**, 26785.
27 K. Heinz and L. Hammer, *J. Phys.:Condens. Matter*, 2013, **25**, 173001.
28 C. Giovanardi, L. Hammer and K. Heinz, *Phys. Rev. B:Condens. Matter Mater. Phys.*, 2006, **74**, 125429.
29 W. Meyer, K. Biedermann, M. Gubo, L. Hammer, *et al.*, *J. Phys.: Condens. Matter*, 2008, **20**, 265011.
30 M. C. Schmidt, J. Smyczek, P. Hubert, M. Cieminski, *et al.*, *Surf. Sci.*, 2024, **742**, 122451.
31 E. M. Davis, A. Bergmann, C. Zhan, H. Kuhlenbeck, *et al.*, *Nat. Commun.*, 2023, **14**, 4791.
32 M. A. Haija, S. Guimond, Y. Romanyshyn, A. Uhl, *et al.*, *Surf. Sci.*, 2006, **600**, 1497.
33 F. E. Feiten, J. Seifert, J. Paier, H. Kuhlenbeck, *et al.*, *Phys. Rev. Lett.*, 2015, **114**, 216101.
34 F. E. Feiten, H. Kuhlenbeck and H.-J. Freund, *J. Phys. Chem. C*, 2015, **119**, 22961.
35 M. Abu Haija, S. Guimond, A. Uhl, H. Kuhlenbeck, *et al.*, *Surf. Sci.*, 2006, **600**, 1040.
36 A. C. Dupuis, M. Abu Haija, B. Richter, H. Kuhlenbeck, *et al.*, *Surf. Sci.*, 2003, **539**, 99.
37 C. Kolczewski, K. Hermann, S. Guimond, H. Kuhlenbeck, *et al.*, *Surf. Sci.*, 2007, **601**, 5394.
38 M. Kratzer, S. Surnev, F. P. Netzer and A. Winkler, *J. Chem. Phys.*, 2006, **125**, 074703.
39 F. P. Leisenberger, S. Surnev, L. Vitali, M. G. Ramsey, *et al.*, *J. Vac. Sci. Technol., A*, 1999, **17**, 1743.

40 S. Surnev, G. Kresse, M. G. Ramsey and F. P. Netzer, *Phys. Rev. Lett.*, 2001, **87**, 086102.
41 S. Surnev, G. Kresse, M. Sock, M. G. Ramsey, *et al.*, *Surf. Sci.*, 2001, **495**, 91.
42 G. Kresse, S. Surnev, J. Schoiswohl and F. P. Netzer, *Surf. Sci.*, 2004, **555**, 118.
43 J. Schoiswohl, M. Sock, S. Surnev, M. G. Ramsey, *et al.*, *Surf. Sci.*, 2004, **555**, 101.
44 Z. Tang, S. Wang, L. Zhang, D. Ding, *et al.*, *Phys. Chem. Chem. Phys.*, 2013, **15**, 12124.
45 S. Guimond, M. Abu Haija, S. Kaya, J. Lu, *et al.*, *Top. Catal.*, 2006, **38**, 117.
46 J. Schoiswohl, M. Sock, S. Eck, S. Surnev, *et al.*, *Phys. Rev. B:Condens. Matter Mater. Phys.*, 2004, **69**, 155403.
47 M. A. Haija, PhD thesis, Fakultät II – Mathematik und Naturwissenschaften der Technischen Universität Berlin, 2006.
48 P. Concepción, H. Knözinger, J. M. López Nieto and A. Martínez-Arias, *J. Phys. Chem. B*, 2002, **106**, 2574.
49 N. Magg, J. B. Giorgi, M. M. Frank, B. Immaraporn, *et al.*, *J. Am. Chem. Soc.*, 2004, **126**, 3616.
50 N. Magg, J. B. Giorgi, A. Hammoudeh, T. Schroeder, *et al.*, *J. Phys. Chem. B*, 2003, **107**, 9003.
51 S. P. Price, X. Tong, C. Ridge, H. L. Neilson, *et al.*, *J. Phys. Chem. A*, 2014, **118**, 8309.
52 J. Kräuter, E. Franz, F. Waidhas, O. Brummel, *et al.*, *J. Catal.*, 2022, **406**, 134.
53 W. X. Huang and J. M. White, *Surf. Sci.*, 2002, **513**, 399.
54 S. C. Street and A. J. Gellman, *J. Phys. Chem. B*, 1997, **101**, 1389.
55 K. A. Davis and D. W. Goodman, *J. Phys. Chem. B*, 2000, **104**, 8557.
56 B. Silvi, P. Labarbe and J. P. Perchard, *Spectrochim. Acta, Part A*, 1973, **29**, 263.
57 E.-T. Es-sebbar, M. Alrefae and A. Farooq, *J. Quant. Spectrosc. Radiat. Transfer*, 2014, **133**, 559.